Structural and Optical Properties of $NdAlO_3$ Nanocrystals Embedded in an Al_2O_3 Matrix

Sanjay Mathur,*,† Michael Veith,*,† Hao Shen,‡ Stefan Hüfner,‡ and Mohammad H. Jilavi§

Institute of Inorganic Chemistry, Institute of Experimental Physics, and Institute of New Materials, Saarland University, D-66041 Saarbruecken, Germany

Received May 20, 2001. Revised Manuscript Received October 8, 2001

Fabrication of an oxide−oxide nanocomposite, containing a homogeneous dispersion of $NdAlO_3$ nanocrystals in an Al_2O_3 matrix, is achieved by employing a single molecular compound, $[NdAl_3(OPr^i)_{12}(Pr^iOH)]$, in the sol−gel process. X-ray diffraction patterns of the composite material show $NdAlO_3$ to be the only crystalline phase, up to 1200 °C, with an equimolar part of amorphous Al_2O_3. The crystallization of alumina (δ-, γ- and κ-phases) occurs at higher temperatures (>1300 °C). TEM investigations reveal a bimodal distribution of particles where $NdAlO_3$ crystallites are uniformly dispersed in an amorphous Al_2O_3 matrix. HR-TEM analysis shows a composite structure formed by $NdAlO_3$ nanocrystals (50−60 nm) homogeneously incorporated in a matrix of smaller alumina particles (10−12 nm). The existence of two chemically different Al(III) species (Al_2O_3 and $NdAlO_3$), in the composite, is proven by ^{27}Al solid-state NMR and XPS studies. The line deconvolution of the Al 2p XPS spectrum reveals two components in a 1:2 ratio with binding energies corresponding to pure $NdAlO_3$ and Al_2O_3. The diphasic nature of the oxide composite is also established by oxygen content analysis. The influence of the alumina matrix on the structural and optical properties of $NdAlO_3$ dispersoids was evaluated by comparing the results of grain growth and photoluminescence of the $NdAlO_3/Al_2O_3$ nanocomposite (**NA3**) with those for a nanocrystalline sample of monophasic neodymium aluminate (**NA**), obtained by the hydrolytic decomposition of the molecular precursor $[NdAl(OPr^i)_6(Pr^iOH)]_2$. The absorption and photoluminescence (PL) spectra of **NA** and **NA3** systems exhibit an enhanced performance in the composite material due to the effect of the $NdAlO_3-Al_2O_3$ interface and the fact that the Al_2O_3 matrix functions as a spacer among the $NdAlO_3$ nanocrystals. The PL efficiency was nearly 35 times higher in **NA3** than in **NA**, which is attributed to the control of the minimum Nd−Nd separation within and on the surface of $NdAlO_3$ nanocrystals coupled with the cooperative energy transfer of the absorbed pumping energy from Al^{3+} to Nd^{3+} ions via the F^+ centers present in the alumina matrix. The results illustrate that the use of *single-source* precursors can impose a strict stoichiometry control at the nanometer scale in monophasic ceramics and a homogeneous dispersion of one phase into another in nanocomposites.

Introduction

It is now well-known that new properties and structures result when crystalline dimensions of matter are reduced to the nanometer regime.[1−5] The inherent advantage of nanostructured materials can be augmented by combining two phases with distinct attributes, resulting in so-called nanocomposites. Such composites suited for important optical applications may be created, for instance, by encapsulating nanocrystals of optically functional phases, in a processable matrix.[6−11] The small particle size enhances the optical properties while the matrix material stabilizes the particle size and prevents random grain growth. The properties of nanocomposites depend, with a reasonable approximation, on the linear combination of the individual characteristics of the two phases and are largely governed by the interfacial interactions between the two components. This permits the growth and design of novel optical materials that would not occur naturally. Recent reports on nanocomposite systems have shown that the matrix materials not only act as passive hosts in sustaining and

* To whom correspondence should be addressed. E-mail: mathur@ch11sgi0.anchem.uni-sb.de; veith@mx.uni-saarland.de.
† Institute of Inorganic Chemistry.
‡ Institute of Experimental Physics.
§ Institute of New Materials.

(1) Gleiter, H. *Acta Mater.* **2000**, *48*, 1.
(2) Hengelein, A. *Chem. Rev.* **1989**, *89*, 1861.
(3) Edelstein, A. S.; Murday, J. S.; Rath, B. B. *Prog. Mater. Sci.* **1997**, *42*, 5.
(4) Edelstein, A. S., Cammarata, R. C., Eds.; *Nanomaterials: Synthesis, Properties and Applications;* Institute of Physics Publishing: Bristol and Philadelphia, PA, 1996.
(5) Fendler, J. H., Ed. *Nanoparticles and Nanostructured Films;* WILEY−VCH: Weinheim, Germany, 1998.
(6) Beecroft, L. L.; Ober, C. K. *Chem. Mater.* **1997**, *9*, 1302.
(7) Tissue, B. M. *Chem. Mater.* **1998**, *10*, 2837.
(8) Blasse, G. *Chem. Mater.* **1989**, *1*, 294.
(9) Carotenuto, G.; Her, Y.; Matijevic, E. *Ind. Eng. Chem. Res.* **1996**, *35*, 2929.
(10) Komarneni, S. *J. Mater. Chem.* **1992**, *2*, 1219.
(11) Kanemitsu, Y.; Tanaka, H.; Kushida, T.; Min, K. S.; Atwater, H. A. *J. Appl. Phys.* **1999**, *86*, 1762.

10.1021/cm0111433 CCC: $22.00
Published on Web 01/16/2002

Scheme 1

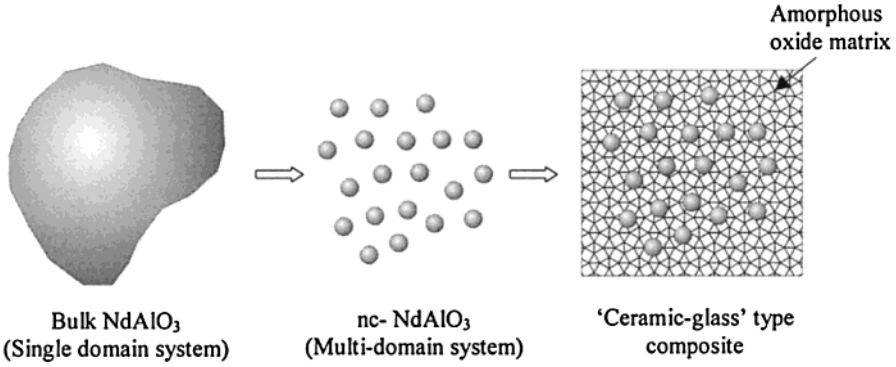

protecting the nanocrystallites but also provide a special environment to the dispersoids.[12−15] For example, the change of the emission peak observed in the CdSe/$BaTiO_3$ composite system has been attributed to the dielectric environment effects of the matrix on the electronic structure of the embedded CdSe quantum dots.

In the context of optical materials, composites containing lanthanide elements or their phases dispersed in an isotropic matrix are of immense technological value and current interest. The neodymium-doped materials are useful as solid-state laser media, phosphors, and optical amplifiers.[6−8,16−18] A general problem encountered in the synthesis of Nd-doped silica glasses is the difficulty to incorporate homogeneously Nd^{3+} ions into a glass matrix because of both physical and chemical limitations. In physical terms, the concentration limitation arises from the proximity of Nd centers giving rise to unfavorable ion−ion interactions, the so-called concentration- or self-quenching identified as a deleterious cross-relaxation process on intermediate levels among the active ions.[19,20] The chemical constraint lies in the limited ability of the pure silica matrix to dissolve large rare earth ions because of the nonavailability of network-forming oxygen atoms.[21−23] The sol−gel process has been successful in producing silica glass with higher dopant concentrations than those for conventional melt glass. However, there is evidence of clustering of the dopant ions in both sol−gel and conventional glasses.[21−23] It has been found that the addition of alumina as a codopant enhances the dispersion of rare earth ions, thus increasing the luminescence efficiency and decay time.[24] The effectiveness of alumina in inhibiting dopant clustering is attributed to the encapsulation of rare earth centers by alumina (coordinative saturation of ill-coordinated Nd sites), which increases the minimum Ln−Ln distance in the material, presumably by forming Ln−O−Al linkages.[25] The present work is based on the concept that if the dopant phase can be added in the form of precursor crystallites with large and fixed Ln−Ln distances, the resulting material could follow a strict positional control on Ln−Ln separation with regularity of a crystalline lattice. By definition, neodymium aluminate belongs to the class of self-activated crystals, like $NdAl_3(BO_3)_4$, which are high gain laser crystals, based on a high Nd concentration.[26] In these crystals, Nd^{3+} ions are not introduced as dopants in a host lattice; instead they constitute the crystalline lattice which allows high Nd concentrations without affecting the optical quality of the material.[26] The intent of this paper is to examine the behavior of $NdAlO_3$ nanocrystals encapsulated in an alumina matrix. Owing to the high surface-to-volume ratio of nanoparticles, a major fraction of the total atoms are situated on the surface of the nanocrystals. The "dilution" (isolation) of surfacial Nd sites by an isotropic medium (matrix) is expected to produce additional Nd-doped Al_2O_3 domains, which can add to the photoluminescence efficiency, when compared to that of the bulk forms of $NdAlO_3$. The phenomenon of neodymium concentration quenching is more likely to occur among Nd centers present in a single domain because the energy transfer (radiative decay) will be favored among closely placed Nd ion pairs. Thus, the loss of excitation energy via concentration quenching will be energetically less favored between Nd ions separated by a grain boundary or an amorphous intergranular medium. Further, the energy absorbed by the alumina matrix can be transferred to the neodymium ions, which can enhance the luminescence efficiency of the material. In view of the above, nanocrystallites of neodymium aluminate reinforced in an amorphous alumina matrix appear to be an attractive ceramic−ceramic composite (Scheme 1). Alumina is suitable as a matrix material due to the following reasons: (i) the crystal structure of alumina enables the incorporation of a high concentration of Nd^{3+} ions by providing them

(12) Fujii, M.; Mimura, A.; Hayashi, S.; Yamamoto, K. *Appl. Phys. Lett.* **1999**, *75*, 184.
(13) Bera, S. K.; Chaudhuri, S.; Pal, A. K. *J. Phys. D: Appl. Phys.* **2000**, *33*, 2326.
(14) Zhou, J.; Li, L.; Gui, Z.; Buddhudu, S.; Zhou, Y. *Appl. Phys. Lett.* **2000**, *76*, 1540.
(15) Bender, C. M.; Burtlich, J. M.; Barber, D.; Pollock, C. *Chem. Mater.* **2000**, *12*, 1969.
(16) Li, H.; Li, L.; Vienna, J. D.; Qian, M.; Wang, Z.; Darab, J. G.; Peeler, D. K. *J. Non-Cryst. Solids* **2000**, *278*, 35.
(17) Ainslie, B. J. *J. Lightwave Technol.* **1991**, *9*, 220.
(18) Campbell, J. H.; Suratwala, T. I. *J. Non-Cryst. Solids* **2000**, *263−264*, 318.
(19) Lupei, V. *Opt. Mater.* **2001**, *16*, 137.
(20) Ikesue, A.; Kamata, K.; Yoshida, K. *J. Am. Ceram. Soc.* **1996**, *79*, 1921.
(21) Campostrini, R.; Carturan, G.; Ferrari, M.; Montagna, M.; Pilla, O. *J. Mater. Res.* **1992**, *7*, 745.
(22) Fujiama, T.; Hori, M.; Sasaki, M. *J. Non-Cryst. Solids* **1990**, *121*, 273.
(23) (a) Bouaziz, J.; Bourret, D.; Sivade, A.; Grill, C. *J. Non-Cryst. Solids* **1992**, *145*, 71. (b) Armellini, C.; Longo, L. D.; Ferrari, M.; Montagna, M.; Pucker, G.; Sagoo, P. *J. Sol−Gel Sci. Technol.* **1998**, *54*, 2133.
(24) Serna, R.; Jimenez de Castro, M.; Chaos, J. A.; Afonso, C. N.; Vickridge, I. *Appl. Phys. Lett.* **1999**, *75*, 4073.
(25) Jaque, D.; Enguita, O.; García Solé, J.; Jiang, A. D.; Luo, Z. D. *Appl. Phys. Lett.* **2000**, *76*, 2176.
(26) Nogami, M.; Abe, Y. *J. Non-Cryst. Solids* **1996**, *197*, 73.

a favorable coordination environment;[27] (ii) it is a suitable amplifying media with a low level of phonon losses;[28] (iii) in comparison to silica, alumina possesses a higher refractive index and optical transparency;[25] and (iv) owing to the well-developed technology of depositing alumina films on silicon chips, it is possible that the compact waveguide devices can be integrated in the nanometer region.

We describe here the successful *single-source* synthesis of (i) monophasic $NdAlO_3$ and (ii) a biphasic $NdAlO_3/Al_2O_3$ composite and investigations on their structural and optical properties. To compare the advantages of the alkoxide processing, the **NA3** composite powder was also synthesized using solid-state and polymeric precursor routes.

Experimental Section

Reagents. Owing to the sensitivity of the alkoxide precursors to atmospheric moisture, the experimental manipulations were performed using a standard vacuum line and modified Schlenk techniques. Hydrocarbon solvents and alcohols were dried using the standard procedures and stored over appropriate desiccating agents. Neodymium(III) chloride (Aldrich) was dried in a vacuum (110 °C/10^{-2} Torr) and analyzed for chlorine content before use. Neodymium alkoxide, $[Nd_3(OBu^t)_9(Bu^tOH)_2]$, was prepared by the reaction of $[Nd\{N(SiMe_3)_2\}_3]$[29] with *tert*-butyl alcohol. Aluminum *tert*-butoxide, $[Al_2(OBu^t)_6]$, was synthesized by reacting Al turnings with Bu^tOH in the presence of small amounts of $HgCl_2$ (catalyst).[30] Analytical grade $Al(NO_3)_3 \cdot 9H_2O$, Al_2O_3, Nd_2O_3, and poly(ethylene glycol) were used as received.

X-ray Crystallography and Instrumentation. X-ray crystallography on the single-crystal specimen of $[NdAl(OPr^i)_6(Pr^iOH)]_2$ was performed on a Siemens Stoe AED 2 diffractometer operating with graphite monochromated Mo Kα X-ray radiation (λ = 0.710 73 Å). Data were collected at room temperature using the $\omega-\theta$ scan technique. The structural analysis was performed using the SHELXS package for the crystal structure solution and refinement.[31] The lattice constants were determined by a least-squares refinement of the setting angles of 25 carefully centered reflections. The data were corrected for Lorentz and polarization effects. A semiempirical absorption correction (ψ-scans) was made. The Nd, Al, and several oxygen atoms could be located directly from the E-map. Further difference Fourier cycles yielded the remainder of the non-hydrogen atoms. All non-hydrogen atoms were refined with anisotropic displacement parameters. Hydrogen atoms were fixed at ideal geometric positions, and their contributions were included in the structural factor calculations.

C, H, and N contents in the gels and calcined powders were determined on a LECO CHN900 elemental analyzer. Room-temperature powder X-ray diffraction patterns were obtained on a STOE diffractometer operating with Cu Kα radiation. The TGA/DTA measurements were performed on a STA 490 analyzer (Netzsch Germany) in quartz/alumina crucibles. The precursors (30−50 mg) were heated (20−1300 °C) in air at a rate of 5 °C/min. The scanning electron imaging (SEM) and energy-dispersive X-ray (EDX) analyses were performed on an EDX coupled scanning electron microscope CAM SCAN S4. The TEM images were recorded on a JEM 200 CX transmission electron microscope. High-resolution electron microscopy was performed on a CM-200 FEG (Philips) transmission electron microscope equipped with a field emission gun operating at 200 kV. The micrographs were recorded with a slow scan CCD camera. The ^{27}Al magic angle spinning (MAS) solid-state NMR spectra were recorded on a Bruker MSL 200 spectrometer using the single-pulse excitation technique. The XPS analyses were performed on a Surface Science instrument (SSI M-Probe) using Al Kα radiation. The total energy resolution of the M-Probe was about 0.8 eV. The peak positions were corrected using residual carbon as the binding energy standard located at +284.6 eV. The light of a 150 W xenon lamp was monochromatized after transmitting it through a double-monochromator (TM300 BENTHAM instrument). The monochromatic light was focused on an integrating sphere, which comprised the sample or a reference material (MgO). The total (combined diffused and specular) hemispherical reflectance was measured in the wavelength range 350−850 nm using an 8° angle of incidence on the powder sample. Since MgO shows no optical absorption in the measured wavelength region, it was used as a standard reference material to determine the spectral function of the instrument. To record the near-infrared emission spectra ($NdAlO_3$ $^4F_{3/2} \rightarrow {}^4I_{9/2}$ emission), a multiline Ar-ion laser operating at 351 nm and 150 mW was used as an excitation source. The IR detector was a liquid-nitrogen-cooled LineSpec CCD. The slits of the optical spectrometer were fixed at 10 μm.

Synthesis and Characterization of Molecular Precursors. The Nd−Al alkoxide, $[NdAl(OPr^i)_6(Pr^iOH)]_2$ (**1**), based on the metal ratio 1:1 was obtained by an equimolar reaction of Nd and Al alkoxides. The neodymium isopropoxide, in-situ generated by the alcoholysis of neodymium tris[bis(trimethylsilyl)]amide, $[Nd\{N(SiMe_3)_2\}_3]$,[29] was reacted with an equivalent of aluminum isopropoxide, in isopropyl alcohol and toluene. The reaction mixture was refluxed (4 h), and the solvent was reduced in a vacuum to obtain lavender blocks of $[NdAl(OPr^i)_6(Pr^iOH)]_2$ in significant yield (70%). The single-crystal X-ray diffraction analysis of **1** established the Nd/Al stoichiometry in the heterometal molecule to be suitable for the $NdAlO_3$ ceramic. The synthesis and X-ray crystallography of $[NdAl_3(OPr^i)_{12}(Pr^iOH)]$ (**2**), used as a single-source for the $NdAlO_3/Al_2O_3$ composite, are described elsewhere.[32] The molecule **1** is a centrosymmetric dimer with its inversion center lying in the middle of the central "Nd_2O_2" ring. The asymmetric unit in **1** constitutes an edge-shared arrangement of a tetrahedron and an octahedron built around Al and Nd atoms, respectively (Figure 1). The Nd(III) atoms achieve an octahedral geometry by the coordination of an additional 2-propanol molecule (O4) while the Al atoms are present in a distorted tetrahedral coordination. A polyhedral representation of the coordination geometries of the metal atoms in **1** and **2** is shown in Figure 2. In contrast to the 7-fold coordination of Nd atoms in **2**, the spatial constraint in **1**, due to the vicinity of two NdO_6 octahedra, limits the coordination of the Nd atoms to an octahedral geometry. The overall molecular structures in **1** and **2** are formed by the bidentate chelation of tetrahedral isopropoxo aluminate group(s) $\{Al(OPr^i)_4\}^-$ to cationic $Nd(OPr^i)_2^+$ and Nd^{3+} fragments, respectively. The Nd and Al arrangements are different in two heterometal frameworks. Whereas **1** shows a Z-conformer (with respect to the arrangement of Nd and Al atoms), a "mitsubishi" motif is formed in **2**. This observation illustrates the structural flexibility of metal alkoxides in forming discrete and isolable entities containing different cation ratios. This ability of component alkoxides to tune the metal stoichiometry according to the need of material of interest also highlights the fact that isolation of the heterometal precursors is important to observe strict control over chemical composition and phase purity in the resulting ceramic material.[33]

(27) Ikesue, A.; Kinoshita, T.; Kamata, K.; Yoshida, K. *J. Am. Ceram. Soc.* **1995**, *78*, 1033.
(28) van der Hoven, G. N.; Koper, R. J. I. M.; Polman, A.; van Dam, C.; van Uffelen, J. W. M.; Smit, M. K. *Appl. Phys. Lett.* **1996**, *68*, 1886.
(29) Lappert, M. F.; Power, P. P.; Sanger, A. R.; Srivastava, R. C. *Metal and Metalloid Amides*; Wiley & Sons: New York, 1980.
(30) Bradley, D. C.; Mehrotra, R. C.; Gaur, D. P. *Metal Alkoxides*; Academic Press: London, 1978.
(31) (a) Sheldrick, G. M. *SHELXS-86, Program for Crystal Structure Determination*; University of Göttingen: Göttingen, 1986. (b) Sheldrick, G. M. *SHELXL-97, Program for Crystal Structure Determination*; University of Göttingen: Göttingen, 1997.
(32) Veith, M.; Mathur, S.; Lecerf, N.; Bartz, K.; Heintz, M.; Huch, V. *Chem. Mater.* **2000**, *12*, 271.
(33) Veith, M.; Mathur, S.; Mathur, C. *Polyhedron* **1998**, *17*, 1005.

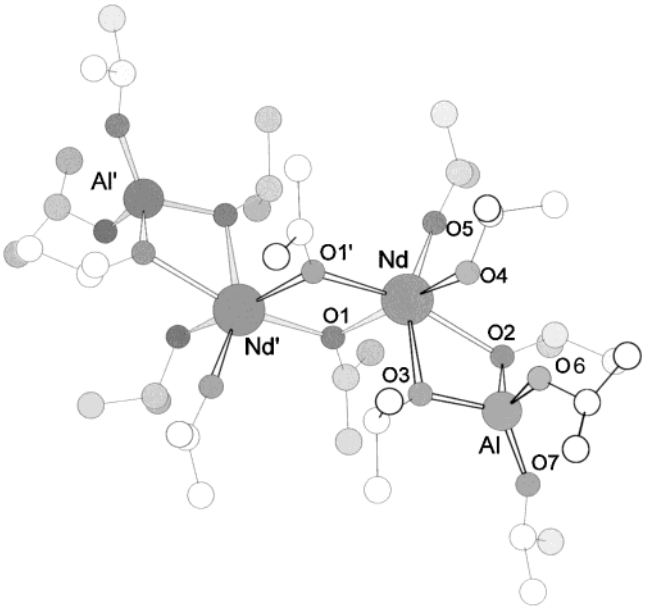

Figure 1. Molecular structure of $[NdAl(OPr^i)_6(PriOH)]_2$ (**1**). Selected bond lengths (Å): Nd−O1, 2.352; Nd−O2, 2.491; Nd−O3, 2.469; Nd−O4, 2.557; Nd−O5, 2.106; Nd−O1′, 2.349; Al−O2, 1.769; Al−O3, 1.767; Al−O7, 1.680; Al−O6, 1.748.

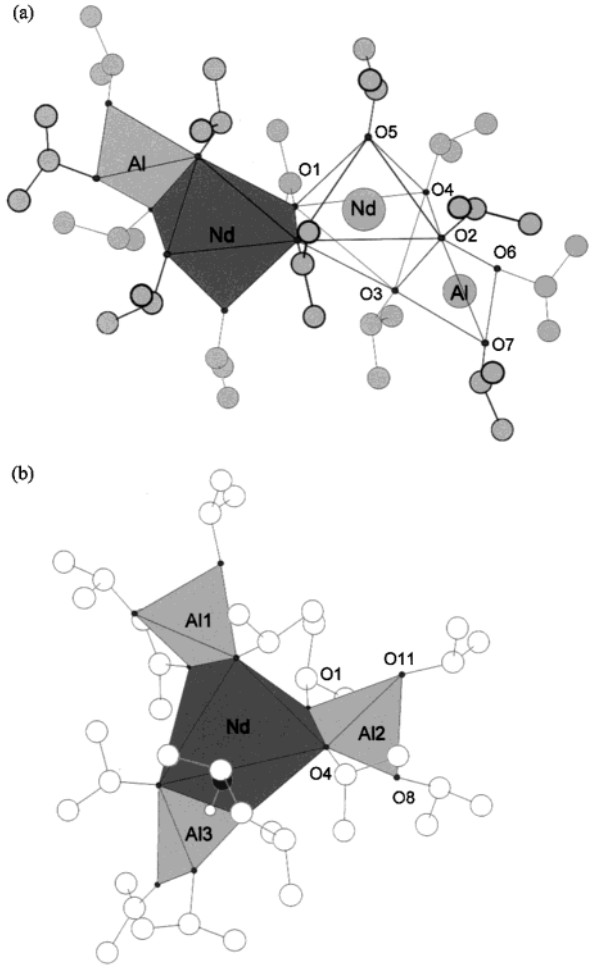

Figure 2. Polyhedral representation of the metal−oxygen frameworks in (a) $[NdAl(OPr^i)_6(Pr^iOH)]_2$ (**1**) and (b) $[NdAl_3(OPr^i)_{12}(Pr^iOH)]$ (**2**).

Nanopowder Synthesis. *(i) Alkoxide Route.* Heterometal alkoxides, $[NdAl(OPr^i)_6(Pr^iOH)]_2$ (Nd/Al = 1:1) (**1**) and $[NdAl_3(OPr^i)_{12}(Pr^iOH)]$ (Nd/Al = 1:3) (**2**), possessing metal ratios suitable for the formation of the $NdAlO_3$ ceramic (**NA**) and the $NdAlO_3/Al_2O_3$ (**NA3**) ceramic−ceramic composite were used as single-source precursors, in the sol−gel process. Both the compounds were subject to controlled hydrolysis to obtain monolithic green bodies. The drying and subsequent firing steps yielded mono- and biphasic nanomaterials according to eqs 1 and 2.

$$[NdAl(OPr^i)_6(Pr^iOH)]_2 \rightarrow NdAlO_3 \quad (1)$$

$$[NdAl_3(OPr^i)_{12}(Pr^iOH)] \rightarrow NdAlO_3/Al_2O_3 \quad (2)$$

In a typical sol−gel synthesis, **1** (or **2**) dissolved in isopropyl alcohol was activated by adding aqueous isopropyl alcohol (3−4 mol of water). In both cases, transparent and purple solutions were obtained after stirring (4−6 h) at 60 °C. The condensation and gelation reactions were faster in the case of **2**, probably because of a higher Al concentration, which enhances the hydrolysis rates. The solutions were allowed to stand, with perforated covers, for several days, which resulted in the formation of monolithic gels, for both the precursor systems. The solvent was removed in a vacuum, and the powders were oven dried (120 °C) to obtain the xerogels. The green powders were calcined (400−1400 °C) in air to obtain the crystalline materials.

(ii) Polymeric Precursor Route. In the polymeric precursor synthesis, the $NdAlO_3/Al_2O_3$ composite was prepared from aqueous sols of the cations and 1,2-ethanediol or poly(ethylene glycol) $(H[OCH_2CH_2]_nOH)$ as the complexing agent (glycolate route) (eq 3).

$$Nd^{3+} + Al^{3+} + \text{(ethylene glycol)} \xrightarrow{H_2O} [-Nd(\text{glycolate})-O-Al(\text{glycolate})-]_n \quad (3)$$

Neodymium oxide was dissolved in an aqueous solution of 0.2 mol/L CH_3COOH, by stirring for 10 h at 60 °C. To this solution was added aluminum nitrate dissolved in 50 mL of distilled water, and the resulting mixture was stirred for 2 h at the same temperature. In a following step, 1,2-ethanediol (25 mmol) was added as a chelating agent to complex the cations. A homogeneous mixing and formation of mixed-metal glycolate precursor(s) was presumed. The acidic medium (pH ∼ 5) is necessary to prevent the flocculation of metal hydroxides in the mixtures. After the solution was concentrated by slow evaporation at 60−70 °C, the Nd−Al acetate−nitrate−glycolate solution turned into a purple transparent gel. The oven dried (100−120 °C) gel became brown due to the initial decomposition of nitrates. The dried powders were ground in an agate mortar and heat treated at 800−1400 °C, in air.

(iii) Solid-State Synthesis. For the solid-state synthesis of the $NdAlO_3/Al_2O_3$ system, appropriate amounts of analytical grade Nd_2O_3 and Al_2O_3 powders were mixed and heat treated at 1000 °C. After several intermediate grinding steps, the powder was heat treated at 1400 °C. The solid-state synthesis was mainly performed to examine the nanometric structure and composition of the oide−oxide composite obtained by the powder processing routes. Thus, the characterization of the sample was limited to EDX and XRD analyses.

Results and Discussion

Precursor Concept. A popular chemical route to produce multicomponent oxide powders is the Pechini-type approach,[34] where a homogeneous precursor cor-

(34) Pechini, M. U. S. Patent No. 3,330,697, 1967.

responding to the target ceramic or composite material is formed by the in-situ complexation of appropriate cations with the help of chelating agents such as poly-hydroxy alcohols (e.g., ethylene glycol) or poly-hydroxy acids (e.g., citric acid). The chemical interactions such as cross-linking of different metal centers within the initial mixture of precursor species are a working assumption. The raw precursor, generally a dense and rigid resin, requires prolonged heat treatments at high temperatures (>1200 °C) and extensive postcalcination grindings to produce the multicomponent oxide.[35−37] The necessity to fire the samples at high temperatures is inevitable to decompose the polymeric starting materials, whereby high disorder, uncontrolled crystal growth, and a high degree of agglomeration are introduced in the powders. In addition, redox processes, inclusion of elemental carbon, and formation of metal carbides are favored too at high temperatures. On the other hand, firing at low temperatures (<1000 °C) leaves a high percentage of carbon impurities in the ceramic material due to an incomplete decomposition of the rather stable intermediates.[36]

The sol−gel synthesis[38−40] using alkoxides is based on inorganic polymerization reactions of partially hydrolyzed alkoxide species that condense and/or link via oxo or hydroxo groups to form multimolecular aggregates (clusters). The major source of organic contamination in the gels is alcohol, which can be easily removed to obtain high-purity materials at low calcination temperatures.[38−40] The method has been widely used in the synthesis of a large number of binary oxides, for example, Al_2O_3, TiO_2, ZrO_2, CeO_2, Nb_2O_5, and so forth. An obvious extension of this strategy to obtain multimetallic ceramics or composites from a mixture of precursors is not straightforward because of the differential hydrolysis behavior of the individual components, often leading to phase separation and formation of unfavorable stoichiometries in the final material. In this context, heterometal alkoxides are a better choice because they supply a controlled and constant flow of reactants in the form of molecular bundles providing an inherent control over particle size and stoichiometry.[41−45]

Characterization of Gels and Powders. *(i) Chemical and EDX Analysis.* The metal ratios and organic contents in the gels and calcined powders were investigated by EDX and chemical analysis. The EDX data show the Nd/Al ratios in the raw powders and the heat-treated samples to be in accordance with the metal stoichiometries present in the precursors **1** and **2**. The Nd and Al contents, randomly checked at different locations (EDX), closely correspond (±1.0%) to the calculated values for the $NdAlO_3$ and $NdAl_3O_6$ compositions. No substantial deviation from the metal ratios or microsegregation of Nd or Al rich grains was observed on a sub-micrometer level, which indicates that a separation into individual metal oxides does not occur in the amorphous gel network. The C and H analysis reveals that the alkoxide-derived gels contain lower organic contents when compared to that of the gel obtained from the glycolate route. The alkoxide powders were free from organic contamination (C, 0.2%; H, 0.04%) after calcination at 900 °C whereas a significant amount of residual carbon was present in the glycolate powders even after firing at 1000 °C (C, 1.2%; H, 0.98%). In contrast to the above, the EDX analysis of the $NdAl_3O_6$ sample prepared by solid-state reaction of Al_2O_3 and Nd_2O_3 showed considerable variations in the Nd/Al ratio and individual Nd_2O_3 (EDX analysis).

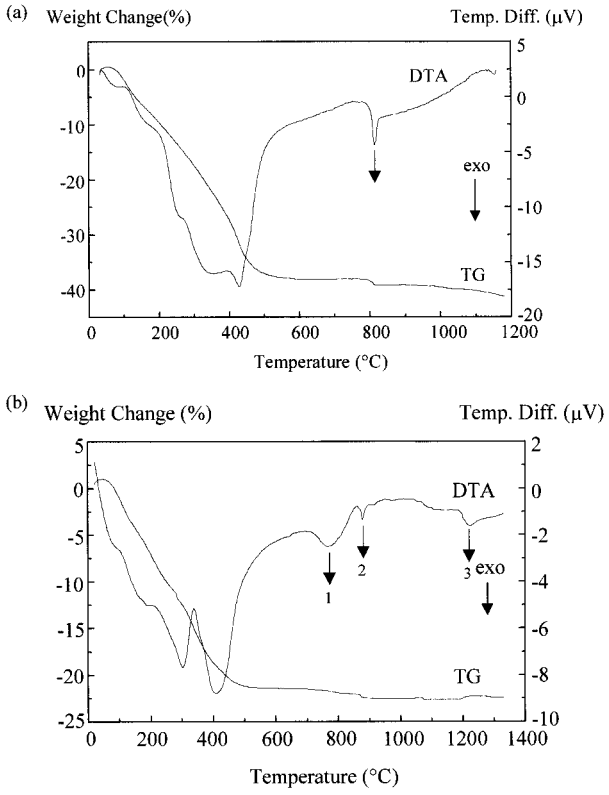

Figure 3. TG/DTA profiles of (a) **NA** and (b) **NA3** xerogels.

(ii) TG/DTA Analysis. The thermal behavior (Figure 3) of **NA** and **NA3** xerogels was investigated by thermogravimetry (TG) and differential thermal analysis (DTA). The DTA trace of the **NA** sample exhibits two endothermic transitions at 110 and 205 °C corresponding to ∼12% weight loss, which are related to the elimination of adsorbed water and alcohol. The major weight loss occurring in the range 205−460 °C is accompanied by two prominent exothermic peaks at 340 and 415 °C ascribable to the oxidative decomposition of the alkoxide ligands. A broad and weak endothermic feature spreading over the range 460−780 °C is probably due to the dehydroxylation process of the residual metal-attached hydroxy groups. Accordingly, no significant weight loss is observed in the TG curve. The sharp exothermic peak at 800 °C indicates the formation of a crystalline $NdAlO_3$ phase, also confirmed by the XRD

(35) Segal, D. *J. Mater. Chem.* **1997**, *7*, 1297.
(36) Veith, M.; Mathur, S.; Kareiva, A.; Jillavi, M.; Zimmer, M.; Huch, V. *J. Mater. Chem.* **1999**, *9*, 3069.
(37) Zayat, M.; Levy, D. *Chem. Mater.* **2000**, *12*, 2263.
(38) Hench, L. L.; West, J. K. *Chem. Rev.* **1990**, *90*, 33.
(39) Chandler, C. D.; Roger, C.; Hampden-Smith, M. J. *Chem. Rev.* **1993**, *93*, 1205.
(40) Mehrotra, R. C. *Chemtracts* **1990**, *2*, 338.
(41) Veith, M.; Mathur, S.; Lecerf, N.; Shen, H.; Huefner, S. *Chem. Mater.* **1999**, *11*, 3103.
(42) Veith, M.; Altherr, A.; Lecerf, N.; Mathur, S.; Valtchev, K.; Fritscher, E. *Nanostruct. Mater.* **1999**, *12*, 191.
(43) Meyer, F.; Hempelmann, R.; Mathur, S.; Veith, M. *J. Mater. Chem.* **1999**, *9*, 1755.
(44) Veith, M.; Mathur, S.; Lecerf, N.; Huch, V.; Decker, T.; Beck, H. P.; Eiser, W.; Haberkorn, R. *J. Sol−Gel Sci. Technol.* **2000**, *17*, 145.
(45) Narula, C. K.; Weber, W. H.; Ying, J. Y.; Allard, L. F. *J. Mater. Chem.* **1997**, *7*, 1821.

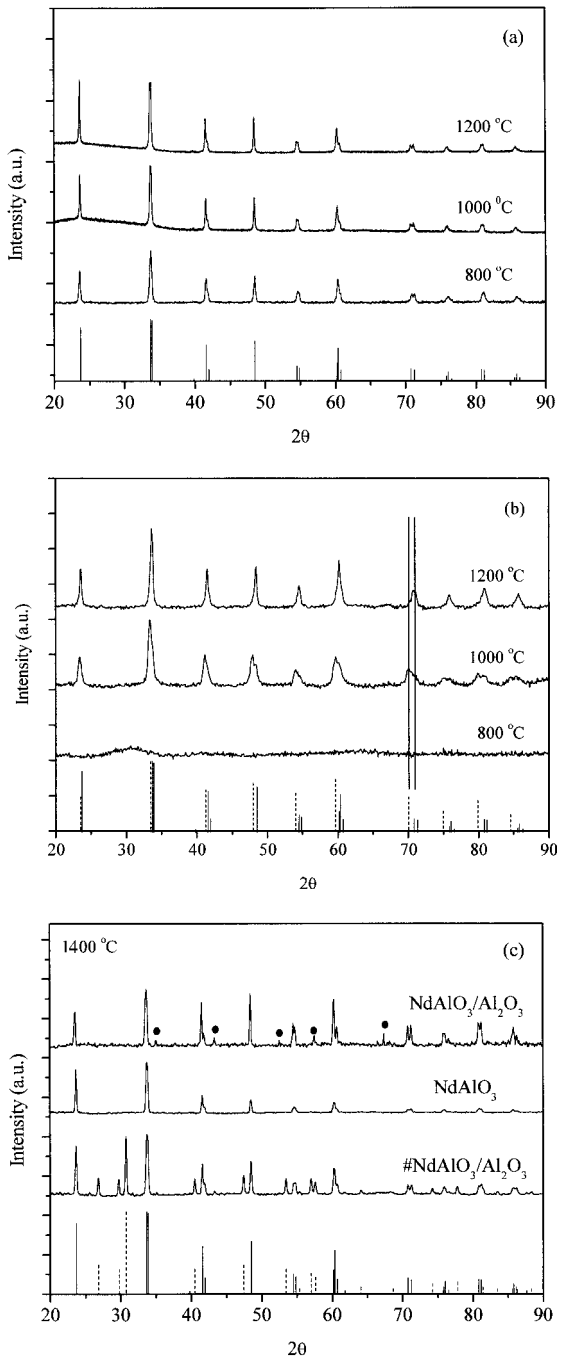

Figure 4. Room temperature X-ray diffractograms of (a) $NdAlO_3$, (b) $NdAlO_3/Al_2O_3$ calcined at 800, 1000, and 1200 °C, and (c) alkoxide-derived $NdAlO_3/Al_2O_3$ and $NdAlO_3/Al_2O_3$ (#) obtained from the solid-state reaction of Nd_2O_3 and Al_2O_3. Solid lines denote rhombohedral $NdAlO_3$, PDF [39-487]; dashed lines in part b denote cubic $NdAlO_3$ PDF [29-56], and Nd_2O_3 in part c PDF [6-408]. The filled circles mark the peaks corresponding to Al_2O_3 phases (mixture of γ, κ, and δ phases).

data (see Figure 4). A small weight loss (~1.2%) accompanying the crystallization of neodymium aluminate is possibly due to the removal of residual hydroxy groups (olation process).

The TG profile of the **NA3** system is essentially similar to that observed for the **NA** system. The TG curves, in both cases, demonstrate that the major weight loss corresponding to thermal decomposition of the precursor occurs in a single step (up to 450 °C), as indicated by prominent exotherms in this region. The decomposition process of the two gels manifests our contention that the single-source properties of the molecular precursors are carried forward to the gels, resulting in the formation of a homogeneous green body with chemically linked Nd and Al centers. The higher temperature region (600−1300 °C) of the DTA trace of the **NA3** system shows three distinct transitions. The broad and intense peak around 800 °C can be assigned to the beginning of the ordering and crystallization processes in the amorphous Nd−O−Al network. The crystallization temperature (870 °C) of neodymium aluminate in the composite powder is higher when compared to that of the monophasic **NA** system (800 °C). The XRD and TEM data indicate that the **NA3** xerogel remains amorphous till 800 °C and the first signs of crystallization are observed at 900 °C. The delayed crystallization of $NdAlO_3$ is probably due to the thermal energy required for the nucleation of $NdAlO_3$ and the associated phase separation. The exothermic peak around 800 °C, in the **NA3** system, is not associated with incipient crystallization of transition aluminas, as the remainder aluminum oxide was shown, by XRD and high-resolution electron microscopy, to be amorphous up to 1200 °C. Indeed, the crystallization of alumina is observed around 1250 °C, as indicated by an exothermic peak in the DTA curve. Since no corresponding weight loss is observed in the TG curve, this transition corresponds to the crystallization of amorphous alumina in the $NdAlO_3/Al_2O_3$ composite.

(iii) Powder X-ray Diffraction Studies. The phase evolution and composition in the **NA** and **NA3** xerogels were established by powder X-ray diffractometry performed on dried gels and heat-treated (600−1400 °C) powders. The xerogels are amorphous in both cases; however, a broad peak in the lower two θ values suggests some local ordering in the gel structure. Using the simple Bragg equation, a rough estimate of the equilibrium distance (X_m) can be made from the angular position (θ_m) of the first maximum of the diffraction pattern (eq 4).[46]

$$X_m = K\lambda/\sin\theta_m \qquad (4)$$

K is a constant with an assumed value of 1.1−1.2. The similar calculated equilibrium distances for **NA** and **NA3** systems (~8−9 Å) indicate a comparable gel structure, in both cases. The equation provides semiquantitative information on the average extension of the first coordination sphere; however, for systems such as **NA** and **NA3** with complex compositions, nothing can be said about the actual occupation of the sites. In the case of the **NA** sample, broad peaks indicating the initiation of the crystallization process are observed around 700 °C. The monophasic $NdAlO_3$ (PDF [39-487], rhombohedral phase)[47] is obtained at 800 °C. The XRD patterns of the material heat treated at 800, 1000, and 1200 °C (Figure 4a) show sharper diffraction profiles corresponding to the continuation of the crystallization process and the faster crystallite growth with increasing temperature, as confirmed by the average crystallite sizes determined by using Scherer's formula. The phase

(46) Lutterotti, L.; Caampostrini, R.; Di Maggio, R.; Gialanella, S. *Mater. Sci. Forum* **2000**, *343−346*, 657.

(47) JCPDS Powder Diffraction File, File Card Nos. [39-487], [29-56], and [6-408]; Joint Committee for Powder Diffraction Standards, 1990.

evolution in the **NA3** system is similar to that observed in the thin films prepared by the chemical vapor deposition (CVD) of $[NdAl_3(OPr^i)_{12}(Pr^iOH)]$;[32] however, the crystallization temperature of the $NdAlO_3$ phase is different in the two cases. Neodymium aluminate crystallizes in the CVD deposits at 800 °C while in the sol−gel synthesis crystallization takes place around 900 °C. This observation can possibly be due to (i) the better ordering of phase-forming atoms, occurring at elevated substrate temperature (500 °C), in a CVD film and/or (ii) the specific decomposition and nucleation mechanisms of the sol−gel and CVD processes. The xerogel obtained from **2** remained amorphous till 850 °C. At 900 °C, $NdAlO_3$ was observed as the only crystalline phase. Further heat treatments up to 1200 °C show neodymium aluminate to be the sole crystalline component. Since the formal composition of the **NA3** system was determined by EDX and chemical analysis to be $NdAl_3O_6$, the residual component was discerned, from stoichiometric balance, to be an equivalent of amorphous aluminum oxide (a-Al_2O_3). This assumption was supported by the partial crystallization of aluminas around 1250 °C (Figure 4c). The crystallization of Al_2O_3 (mixture of γ, κ, and δ phases) phases becomes more evident at higher temperature. Figure 4c compares the diffraction patterns of the **NA** and **NA3** nanopowders after heat treatment at 1400 °C. Whereas the **NA** powder shows reflections, which can be exclusively indexed to the $NdAlO_3$ phase, additional peaks corresponding to the alumina fraction are observed in the **NA3** powder. A similar observation was made for the powder synthesized by the glycolate route; however, despite the fact that a biphasic configuration of the two oxides was obtained, the microstructure of the material was different (see TEM analysis). The particles show (Figure 11) strong agglomeration effects, and it is not possible to differentiate the primary particles ($NdAlO_3$) from the matrix. In contrast to the above, the powder obtained from the solid-state reaction between Al_2O_3 and Nd_2O_3 showed (after repeat grinding and firing (1000−1400 °C) steps) $NdAlO_3$ and Nd_2O_3 as the only crystalline phases (Figure 4c: PDF [39-487], solid line; PDF [6-408], dashed line) and an amorphous component (XRD profile).

It is interesting to note that, in the **NA3** powder calcined at 1000 °C, a mixture of cubic (PDF [29-56]) and rhombohedral (PDF [39-487]) $NdAlO_3$ phases is present. The cubic form predominates at lower temperature; however, a nonreversible cubic → rhombohedral phase transition occurs at higher temperatures (1200−1400 °C, Figure 4b). In Figure 4b, the cubic and rhombohedral phases are shown as dashed and solid lines, respectively. In the case of pure $NdAlO_3$ no phase transition is observed in going from the nanometer to the micrometer regime and the thermodynamically favored phase (rhombohedral) is formed from the beginning of the crystallization. It should be noted that the formation of phases not possessing the lowest free energy, which characterizes thermodynamic stable phases, is often observed in soft chemistry methods. The number of atoms present on the surface layers of a nanoparticle increases with decreasing particle size. Such atoms experience an unbalanced surface stress and tend to migrate to more stable positions for reducing the total surface energy. In general, the surface atoms migrate to achieve an isotropic coordination with higher symmetry. The dangling bonds of the surface atoms of $NdAlO_3$ can bond to the alumina matrix, which can influence the structure and symmetry of the $NdAlO_3$ grains. This is more likely at temperatures below 1000 °C, before the microphase separation begins. This can explain the observed cubic form for the very small $NdAlO_3$ crystallites. According to the experimental data, below a critical particle size (<20 nm) the rhombohedral and the higher symmetry phases (cubic) coexist; however, for bigger particle size the magnitude of the lattice distortion is governed by thermodynamics, which outweighs the tendency of surface atoms to decrease the total free energy of the system (entropy rules!), resulting in the formation of the rhombohedral structure observed for the bulk neodymium aluminate. Since the initial average crystallite size observed for the pure $NdAlO_3$ phase (∼42 nm) is much higher than the critical particle size required for the cubic phase, only the rhombohedral form is observed in the monophasic system. The temperature dependence of the structures and the phase transitions of $NdAlO_3$ have been examined by Coutures and Coutures[48] between room and melting temperatures via X-ray diffraction experiments. The results indicate that the room temperature rhombohedral structure undergoes a second-order phase transition to the ideal cubic phase at high temperature (∼1500 °C). In our studies, an inverse phase transition (cubic → rhombohedral) is observed to occur at lower temperature (∼1000 °C) in the composite system. The existence of a high-temperature phase in the **NA3** sample, calcined at lower temperature, can be attributed to strong surface tension due to many dangling bonds in small particles, which favors a compact structure (cubic).

The broadening of the full-width at half-maximum (fwhm) of the diffraction peaks can be used to obtain the average particle size in nanocrystalline samples (Scherer's formula), provided the size dispersion of crystallites is not too broad. The volume-weighted average crystallite size (XRD) in our samples was close to that found in the TEM observations (see following section). Figure 5 displays the average crystallite sizes (D_m), of $NdAlO_3$ grains in the **NA** and **NA3** systems plotted against the calcination temperatures. As expected, the grains in pure $NdAlO_3$ powder experience a continuous (exponential) growth whereas, in the $NdAlO_3$/Al_2O_3 composite system, the growth of $NdAlO_3$ crystallites is restricted due to the presence of a second phase. The average crystallite size of $NdAlO_3$ at a particular calcination temperature is significantly larger in the single-phase system. This is due to the influence of second-phase particles (alumina), which retard the kinetics of the grain growth through grain boundary pinning. In contrast to the exponential growth observed for the **NA** system, the temperature dependence of the grain growth in the **NA3** composite shows two distinct regions (Figure 5, parts a and b). In the composite sample, the grain growth is faster below 1200 °C but slows down considerably above this temperature. In the temperature range 800−1200 °C (part a), the nucleation and growth of neodymium aluminate crystallites in an

(48) Coutures, J.; Coutures, J. P. *J. Solid State Chem.* **1984**, *52*, 95.

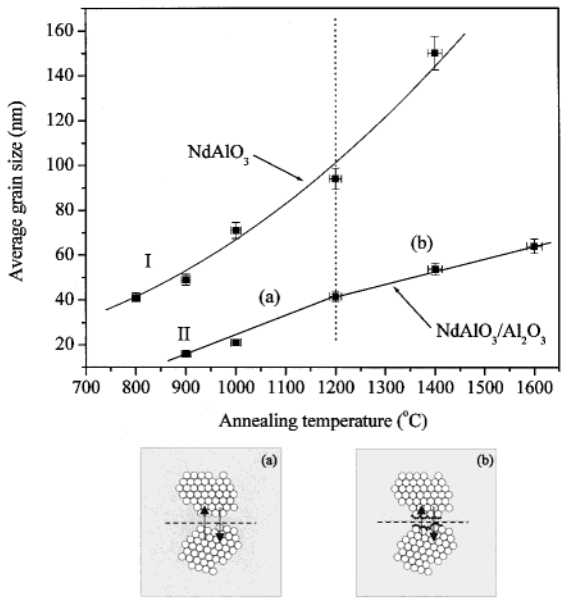

Figure 5. Dependence of the crystallite size on the calcination temperature in $NdAlO_3$(I) and the $NdAlO_3/Al_2O_3$(II) composite. The adjacent scheme shows the physical models of the grain growth processes in amorphous and crystalline states of the matrix in the **NA3** system and corresponds to the two regimes a and b (curve II).

amorphous aluminum oxide medium takes place but slows down at higher temperature probably because of the different diffusion rates. Moreover, the alumina, in view of its higher thermal conductivity,[49,50] may function as a microcrucible and conduct heat to the embedded $NdAlO_3$ nanocrystallites, thereby providing the activation energy necessary for grain growth of $NdAlO_3$. Thus, the "crucible effect" is a combination of both the higher thermal conductivity of alumina (which rapidly transfers the thermal energy to the encapsulated $NdAlO_3$ grains) and the higher heat capacity of neodymium aluminate to accumulate the heat. The mechanism of thermal energy transfer from the matrix to the embedded crystallite may be attributed to a reduction of the total surface energy of the composite. The competition between $NdAlO_3$ and alumina particles for the externally provided thermal energy results in the delayed crystallization of alumina (~1250 °C, against the reported crystallization temperature ~750 °C for nanoscaled alumina[51]). In addition, the different crystallization temperatures of $NdAlO_3$ are also indicated in the TG/DTA profiles of the two systems (~870 °C in the $NdAlO_3/Al_2O_3$ composite against 800 °C for $NdAlO_3$). The further restricted grain growth of the $NdAlO_3$ phase in the second regime (Figure 5, part b) is associated with the crystallization of alumina nanoparticles, which may adhere to the surface of the $NdAlO_3$ crystals, forming a dense oxide shell, thereby inhibiting the percolation of ions and impeding the grain growth. This observation shows that the presence of a crystalline matrix can sustain the aggregation and abnormal growth of nanocrystals, at higher temperatures.

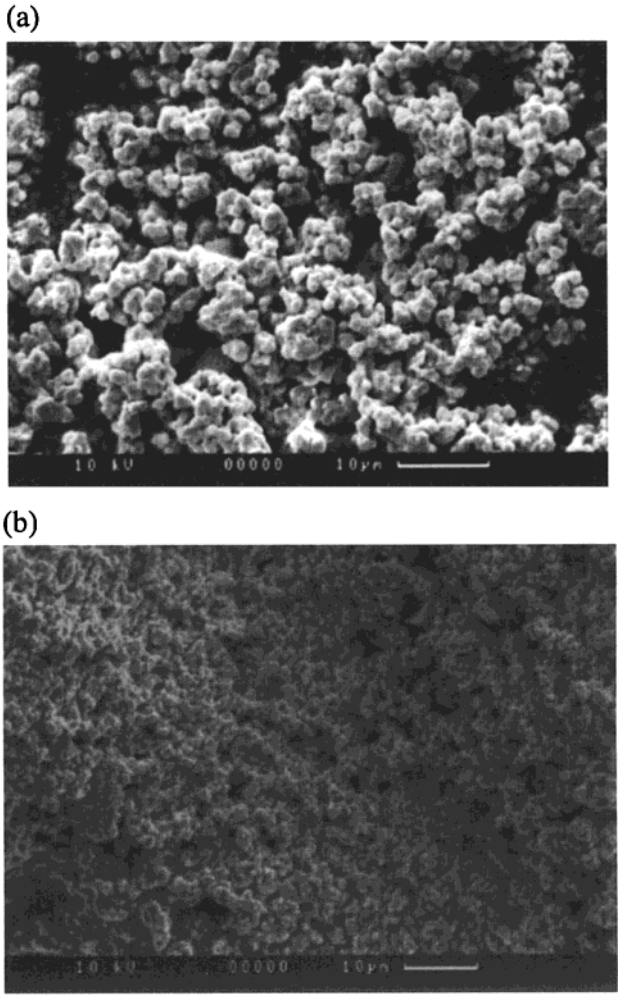

Figure 6. SEM images of the calcined (1000 °C) gels obtained from the hydrolysis of (a) $[NdAl(OPr^i)_6(Pr^iOH)]_2$ (**1**) and (b) $[NdAl_3(OPr^i)_{12}(Pr^iOH)]$ (**2**).

(iv) Electron Microscopy. The scanning electron micrographs of **NA** and **NA3** xerogels (not shown) revealed interconnected porous microstructures with a morphology typical for alkoxide-derived gels.[36] The SEM images of the calcined (1000 °C) gels show agglomerated grains with a globular microstructure (Figure 6). The particle size was found to be significantly larger for the **NA** system. Further, the strong agglomeration of particles indicates the begining of the sintering process in the **NA** powder. To examine the sintering behaviors of the two systems, the calcined powders of $NdAlO_3$ and $NdAlO_3/Al_2O_3$ synthesized from both alkoxide and glycolate routes were uniaxially pressed (10 MPa) and sintered in air at 1200 °C. Figure 7 shows the cross-sectional view of a pure $NdAlO_3$ compact, which exhibits a dense fracture surface constituted of uniform grains sintered together. There are no signs of intragranular or intergranular porosity. The narrow size distribution and compositional purity of the grains (free from secondary phases and organic contamination) is responsible for the compact structure and high densification at relatively low temperature (1200 °C). On the contrary, the fractograph of the $NdAlO_3/Al_2O_3$ compact (alkoxide powder) reveals a bimodal microstructure made up of large faceted grains and smaller spherical

(49) (a) van der Laan, R. R.; Konings, R. J. M.; van Genderen, A. C. G.; van Miltenburg, J. C. *Thermochimica* **1999**, *329*, 1. (b) Morelli, D. T. *J. Mater. Res.* **1992**, *7*, 2492.

(50) (a) Lide, D. R. *CRC Handbook of Chemistry and Physics*, 78th ed.; CRC Press: Boca Raton, FL, 1997−1998. (b) Shoup, S. S.; Paranthaman, M.; Goyal, A.; Specht, E. D.; Lee, D. F.; Kroeger, D. M.; Beach, D. B. *J. Am. Ceram. Soc.* **1998**, *81*, 3019.

(51) Urretavizacya, G.; Cavalieri, A. L.; Porto Lopez, J. M.; Sobrados, I.; Sanz, J. *J. Mater. Synth. Process* **1998**, *6*, 1.

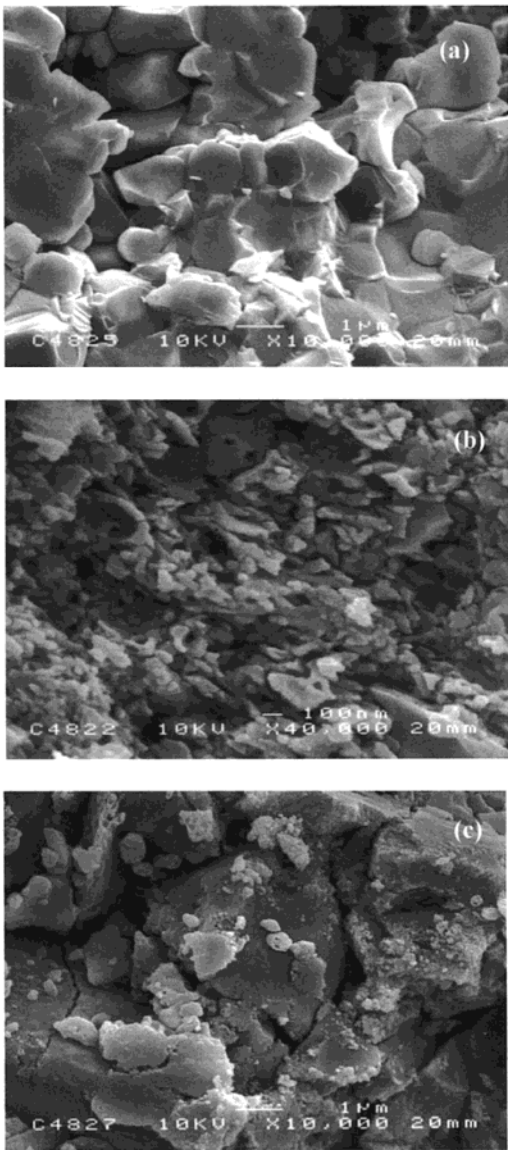

Figure 7. SEM cross section images of compacts (1200 °C) of **NA** (a), **NA3** (b), and a $NdAlO_3/Al_2O_3$ sample obtained from a multisource (c).

particles, which fill the voids generated by the larger crystals. The faceted particles were shown, by micro-EDX analysis, to be $NdAlO_3$ grains whereas the agglomerates of spherical grains mainly contain Al and O (EDX). The preferential crystallization and growth of $NdAlO_3$ crystals (XRD and TEM evidences) is also confirmed in the SEM analysis by their bigger size and faceted structure when compared to the grain size and form of the Al_2O_3 particles. In multiphase materials, the emergence of crystallization and/or the ordering process of the secondary phase(s) can restrain the grain growth of the main phase necessary for the densification process. In the **NA3** system, amorphous Al_2O_3 acting as a second phase inhibits the growth of $NdAlO_3$. Consequently, the $NdAlO_3/Al_2O_3$ system is less dense than pure $NdAlO_3$ after sintering under identical conditions. On the other hand, the powder obtained from the glycolate precursor exhibits a packing of large grains with a number of small particles sticking on them (Figure 7). Also, a number of cracks and voids are observed. Although the XRD data show only $NdAlO_3$ to be the crystalline component in the $NdAlO_3/Al_2O_3$ synthesized from the multicomponent process, the two phases are not distinguishable on the basis of the grain form and the crystal textures. This observation is further corroborated by the TEM image of the composite powder obtained from the polymeric precursor (see below).

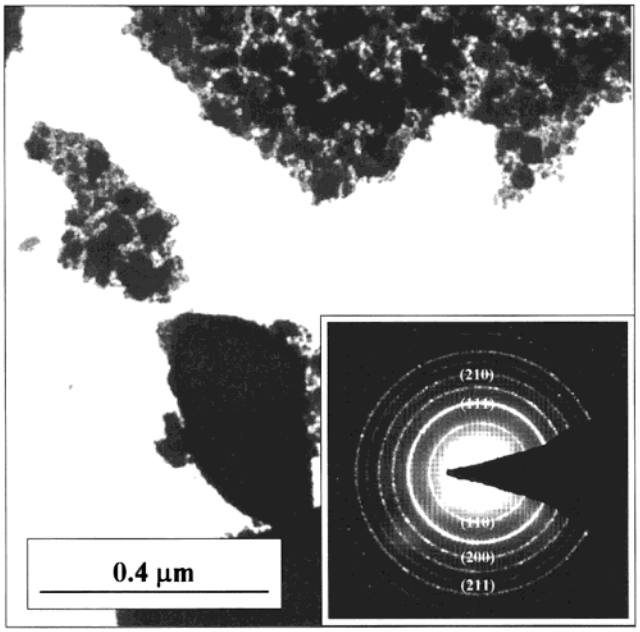

Figure 8. TEM image and corresponding electron diffraction pattern for $NdAlO_3/Al_2O_3$ composite powder.

The TEM image of the **NA3** system revealed that the nucleation of $NdAlO_3$ particles in an amorphous matrix begins around 900 °C. The material at this stage is largely homogeneous with some phase-separated domains. The TEM image (Figure 8) of a sample heat treated at 1200 °C shows a bimodal distribution of $NdAlO_3$ nanocrystals in a matrix made up of small crystallites. The selected area electron diffraction (SAED) pattern (inset, Figure 8) of the sample shows a set of rings instead of spots, as expected for randomly oriented nanocrystallites. The principal rings (Figure 8) correspond to the (110), (111), (200), (210), and (211) planes of the rhombohedral $NdAlO_3$ phase. The calculated lattice spacings are in agreement with the reported $NdAlO_3$ structure. The biphasic structure is clearly observed in the TEM image (Figure 9b) of the $NdAlO_3/Al_2O_3$ composite powder fired at 1400 °C, which shows equiaxed grains of $NdAlO_3$ (∼55 nm) regularly dispersed in an alumina matrix made up of tiny crystallites (∼10 nm). The micro-EDX analysis of the individual crystallites confirmed the bigger particles to be $NdAlO_3$ crystals, while the smaller grains have the alumina composition. The $NdAlO_3$ nanocrystallites exist as isolated domains in the Al_2O_3 matrix with no overlap between neighboring particles. No chemical reaction is observed between the two phases even upon sintering at high temperatures (1400 °C).[52] It is noteworthy that the fabrication of $NdAlO_3/Al_2O_3$ composite from a single source precursor opens up a new dimension in the synthesis of biphasic ceramic−ceramic composites, which, despite an ultrahomogeneous mixing at the nanometer scale, exist as discrete phases at higher temperatures (nanoheterogeneity). The high-resolution TEM image (Figure 10) of the **NA3** powder calcined at 1400 °C

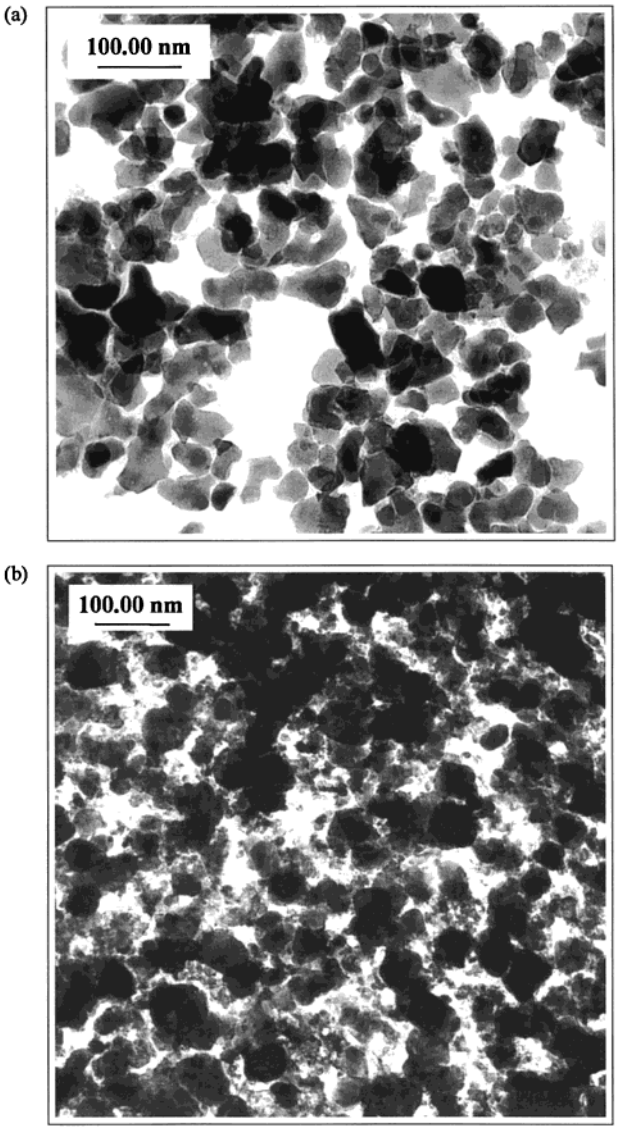

Figure 9. TEM images of (a) $NdAlO_3$ and (b) $NdAlO_3/Al_2O_3$ samples calcined at 1000 and 1200 °C, respectively.

shows crystalline $NdAlO_3$ domains with well-defined lattice fringes dispersed among Al_2O_3 crystallites. The TEM image of the single-phase $NdAlO_3$ ceramic (Figure 9a), heat treated at 1000 °C, shows dispersed crystallites with an average size of about 70 nm. No distinct morphology is observed, probably because of the grain boundary fusion and the onset of the sintering process. The crystallite growth via grain boundary fusion is observed in the neck-formation of small $NdAlO_3$ crystallites forming dumbbell-shaped particles.

The microstructure of the $NdAlO_3/Al_2O_3$ composite powder prepared via the glycolate route was also investigated by transmission electron microscopy. Similar to the case of alkoxide-derived powders, the SAED pattern shows $NdAlO_3$ to be the only crystalline component, which is also supported by the powder X-ray diffraction data. The TEM micrograph (Figure 11), however, shows a high degree of agglomeration in the sample with grains formed by clustering of nanoparticles of different sizes. Despite the similar overall composition and crystalline−amorphous nature, the two $NdAlO_3/Al_2O_3$ composites differ significantly in the microstructure. This is an important aspect, particularly

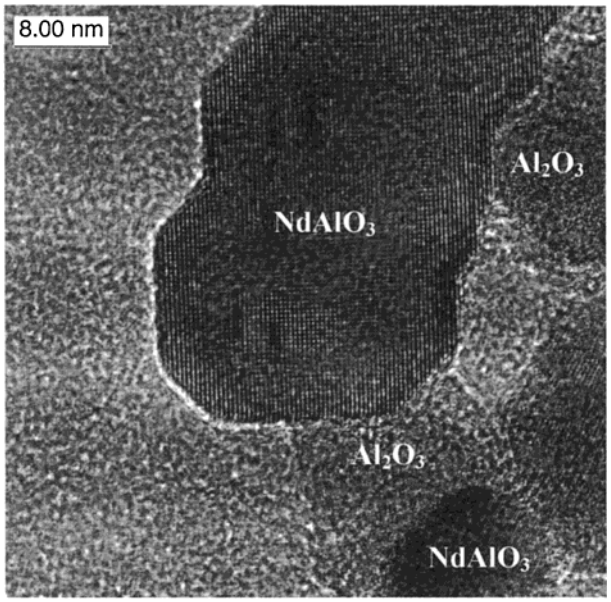

Figure 10. HR-TEM image of $NdAlO_3/Al_2O_3$ composite calcined at 1400 °C.

in the context of functional composites. In an earlier investigation,[36] we have shown that the powders obtained from the polymeric precursor route contain a significant amount of residual carbon, which acts as a binder present in the grain boundary regions to form large interparticle aggregates.

(v) ^{27}Al NMR Spectroscopy. The local environment (Al−O coordination) of the Al^{3+} cations in multiphase alumina-based materials can be determined by ^{27}Al magic angle spinning nuclear magnetic resonance (MAS NMR).[53−56] The ^{27}Al NMR spectrum (Figure 12a) of monophasic $NdAlO_3$ is characterized by a sharp resonance maximum at 7.62 ppm corresponding to Al(III) centers in 6-fold coordination with oxygen. The main signal is flanked by broad shoulders that comprise the spinning sidebands. The sidebands are not well formed because of the nanocrystalline nature of the sample. The NMR spectrum of the $NdAlO_3/Al_2O_3$ composite exhibits three signals assignable to Al(III) centers present in different chemical surroundings: (i) a central transition at 8.90 ppm, characteristic for octahedrally coordinated Al atoms (AlO_6 site), (ii) a shoulder at 48.7 ppm, which is not resolved from the AlO_6 resonance, and (iii) a broad peak (∼110−135 ppm) corresponding to tetracoordinated Al centers. The signal due to 4-fold coordinated Al centers overlaps with the first-order spinning sidebands of the central transition; however, the contribution of tetracoordinated Al(III) centers has been confirmed by line deconvolution and peak fitting procedures. In light of other analytical results, the occurrence of additional peak(s) in the composite powder is probably due to the amorphous alumina phase, containing 4-, 5-,

(52) Deschanvres, J. L.; Meffre, W.; Joubert, J. C.; Senateur, J. P.; Robaut, F.; Broquit, J. E.; Rimet, R. *J. Alloys Compd.* **1998**, *275*, 742.
(53) Gerardin, C.; Sundaresan, S.; Benziger, J.; Navrotsky, A. *Chem. Mater.* **1994**, *6*, 160.
(54) Sanz, J.; Madani, A.; Serratosa, J. M.; Moya, J. S.; Aza, S. *J. Am. Ceram. Soc.* **1988**, *71*, C418.
(55) Balmer, M. L.; Eckert, H.; Das, N.; Lange, F. *J. Am. Ceram. Soc.* **1996**, *79*, 321.
(56) Bonhomme-Coury, L.; Babonneau, F.; Livage, J. *Chem. Mater.* **1993**, *5*, 323.

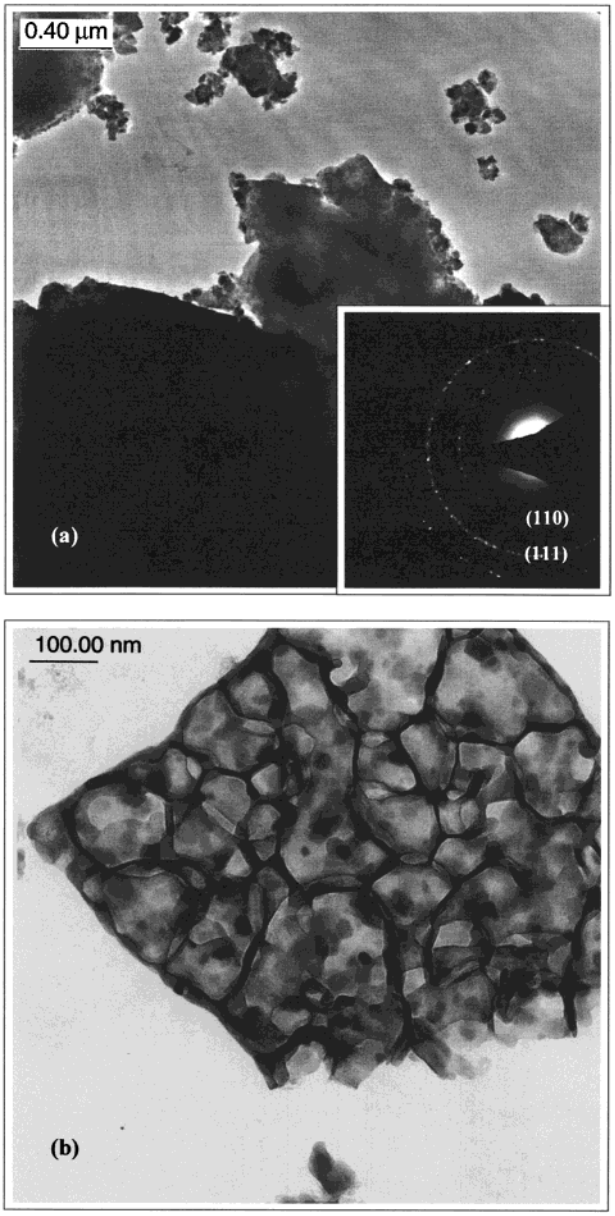

Figure 11. Transmission electron micrographs of the $NdAlO_3/Al_2O_3$ composite obtained from a multisource precursor.

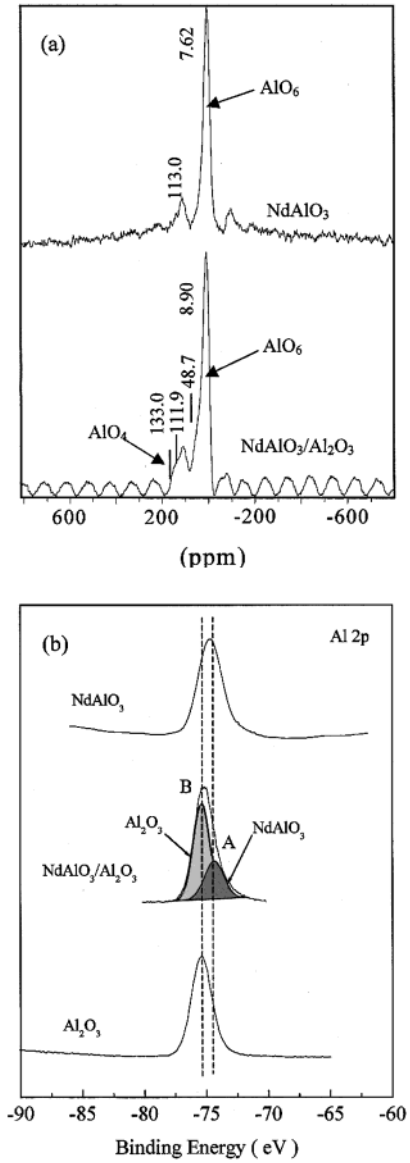

Figure 12. (a) ^{27}Al solid-state MAS NMR spectra and (b) Al 2p XPS spectra of $NdAlO_3$ and $NdAlO_3/Al_2O_3$.

or 6-coordinated aluminum sites. The peak heights of the NMR signals do not correlate with the Al_2O_3 mole fraction present in the **NA3** powder because the intensity of the resonances is significantly affected by the symmetry of the Al(III) coordination geometry and the crystallinity of the sample. Further, the ^{27}Al isotropic shift is affected because of the next-nearest neighbors. A similar observation has been made in the ^{27}Al MAS NMR spectra of the $PrAlO_3/Al_2O_3$ composite prepared by chemical vapor deposition.[57]

(vi) X-ray Photoelectron Spectroscopy. X-ray photoelectron spectroscopy (XPS) was used to determine the chemical composition of the **NA** and **NA3** systems and to corroborate the existence of two chemically different Al species, in the **NA3** system. The elemental stoichiometries (Nd/Al/O) in the **NA** and **NA3** systems were determined to be $NdAl_{1.02}O_{2.95}$ and $NdAl_{2.96}O_{5.88}$, respectively. Figure 12b shows the Al 2p peaks of nanocrystalline samples of $NdAlO_3$, $NdAlO_3/Al_2O_3$, and Al_2O_3. The nanoscaled alumina, used as a reference sample, was prepared by the sol−gel synthesis using $[Al(OPr^i)_3]_4$ as precursor. The Al 2p peaks in $NdAlO_3$ and Al_2O_3 are observed as single peaks at binding energies of +74.7 and +75.4 eV, respectively. However, the Al 2p peak in $NdAlO_3/Al_2O_3$ shows an asymmetrical profile with a shoulder observed on the low E_b side. The deconvolution of the Al 2p peak resulted in two Gaussian components with an intensity ratio 1:2 (Figure 12b, A and B). On the basis of the chemical binding energy differences, the two peaks present at E_b = 74.3 and 75.4 eV can be assigned to the $NdAlO_3$ and Al_2O_3 phases, respectively.

(vii) Oxygen Analysis. To eliminate the possible coexistence of other Nd/Al/O stoichiometries in the samples, the oxygen contents of the **NA** and **NA3** powders were analyzed (Figure 13). The decomposition of the oxide samples was investigated in ramping mode by stepwise increasing the temperature to 3000 °C. The oxygen liberated at the decomposition temperature reacted with the graphite sample holder to form carbon

(57) Veith, M.; Mathur, S.; Hao, S.; Lecerf, N.; Hüfner, S.; Jilavi, M. *Chem. Mater.* **2001**, *13*, 4041.

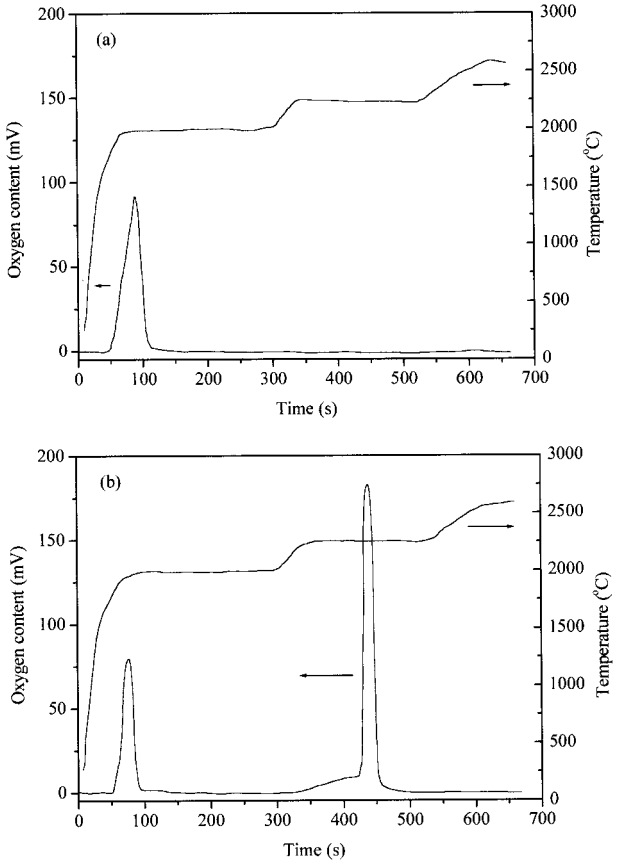

Figure 13. Oxygen content analysis of (a) $NdAlO_3$ and (b) $NdAlO_3/Al_2O_3$.

monoxide (CO), which was quantitatively detected by the infrared absorption. The concentration of liberated CO, the blank reading (empty sample holder), and the weight loss of the sample gave the oxygen content (wt %) in the sample. Since each oxide possesses a characteristic decomposition temperature, the method is reliable in analyzing oxide−oxide composites. Figure 13a shows the oxygen analysis profile for the **NA** system where a single peak observed at 2070 °C represents the thermal decomposition of neodymium aluminate. On the other hand, the **NA3** composite revealed two distinct peaks at 2050 and 2350 °C corresponding to the decomposition of the $NdAlO_3$ and Al_2O_3 phases. The above values closely correspond to the melting points (mps) of the two phases, which rules out the presence of other compounds such as $NdAl_{11}O_{18}$ (mp, 1795 °C) and $Nd_2Al_4O_9$ (mp, 1905 °C), observed in the Nd_2O_3/Al_2O_3 phase diagram.[52,58] The integral area of the two peaks (1:2.21) approximately corresponds to the ratio of the calculated oxygen contents (1:2.15), implying that only $NdAlO_3$ and Al_2O_3 are present in the **NA3** system, a fact borne out by the XRD, TEM, NMR, and XPS results.

Optical Properties. *(i) Absorption Spectra.* The room temperature absorption spectra (Figure 14) of the $NdAlO_3$ and $NdAlO_3/Al_2O_3$ systems recorded in the UV−vis region (350−850 nm) show the characteristic Stark splitting of the degenerate 4f levels of Nd^{3+} ion in a crystal field.[59−62] The absorption features of the singular **NA** phase and the **NA3** composite appear to be similar because (i) the observed Stark levels represent the intrinsic picture of the electronic transitions of partially filled Nd 4f energy levels and (ii) the fact that the absorption of alumina is featureless in the recorded wavelength region. Moreover, the 4f electrons of each Nd ion are shielded by the outer-shell 5s and 5p electrons, which makes the Nd^{3+} energy levels independent of their surroundings. Nevertheless, the absorption coefficients for the transition from the $^4I_{9/2}$ ground state to higher excited states ($^4F_{9/2}$ or $^2H_{11/2}$ or $^2G_{7/2} + {}^2G_{5/2}$ or $^2K_{13/2} + {}^4G_{7/2} + {}^2G_{9/2}$) are significantly larger in the $NdAlO_3/Al_2O_3$ composite than in single-phase $NdAlO_3$, although the absorption coefficients of the $^4F_{7/2} + {}^4S_{3/2}$ and $^2H_{9/2} + {}^4F_{5/2}$ bands in the two systems are comparable (Figure 14). The composite **NA3** shows a nonlinear enhancement of the absorption coefficient in the UV−vis region (<700 nm), which is nearly 2−3 times larger in the visible range. Since the main difference between the **NA** and **NA3** samples is the presence of alumina in the latter, the electronic structure of the Nd^{3+} ions situated on the surface of $NdAlO_3$ crystals is probably affected because of their bonding to several Al_2O_3 clusters. The enhanced absorption of the composite is of interest because in order to obtain a gain element of small dimensions (e.g., microchip lasers) materials with high absorption coefficients (high Nd concentration) are needed.

The influence of the Al_2O_3 matrix becomes evident in the high-resolution absorption spectra of both systems recorded at 10 K. The $^4I_{9/2}(1) \rightarrow {}^4F_{9/2}(1)$ transition (675−692 nm), for both systems, is shown in Figure 15. The $NdAlO_3$ spectrum shows a single peak and a shoulder (M), whereas the $NdAlO_3/Al_2O_3$ composite exhibits, besides the main peak N, a series of satellites (P_x). The main line N corresponds to Nd^{3+} ion in a nonperturbed $NdAlO_3$ structure, and the P_x peaks in the composite are attributed to perturbed $NdAlO_3$ and Nd/Al_2O_3 phases.[63] The HR-TEM studies have shown that the $NdAlO_3$ nanocrystals are densely surrounded by many tiny Al_2O_3 crystallites. A possible substitution of some of the Al^{3+} ions by Nd^{3+} or vice versa in the interface region may distort the local symmetry and thereby the crystal field experienced by the Nd ions present on the surface of $NdAlO_3$ crystallites. Any such perturbation can cause a shift in the energy levels of the Nd ion, leading, in addition to the main line N, to satellites P_x in the high-resolution spectra (Figure 15).[63]

(ii) Photoluminescence Spectra. Figure 16 shows the photoluminescence (PL) spectra of the two systems excited at 4 K by 351 nm radiation (Ar ion laser). When compared to the PL spectrum of $NdAlO_3$, an enhanced (35×) PL intensity is observed for the $NdAlO_3/Al_2O_3$ sample. In view of the observed higher absorption coefficient and photoluminescence of the **NA3** sample, it is reasonable to assume that the energy transfer from the alumina matrix to the Nd^{3+} cations is operative in the composite material. The surface defects in the

(58) Coutures, J. P. *J. Am. Ceram. Soc.* **1985**, *68*, 105.
(59) Kushida, T.; Macros, H. M.; Geusic, J. E. *Phys. Rev.* **1968**, *167*, 289.
(60) Rukmini, E.; Jayasankar, C. K. *Physica B* **1995**, *212*, 167.
(61) Antic-Fidancev, E.; Lemaitre-Blaise, M.; Beaury, L.; Teste de Sagey, G.; Caro, P. *J. Chem. Phys.* **1980**, *73*, 4613.
(62) Finkman, E.; Cohen, E.; Van Uitert, L. G. *Phys. Rev. B* **1973**, *7*, 2899.
(63) Lupei, V.; Lupei, A.; Tiseanu, C.; Georgescu, S.; Stoicescu, C.; Nanau, P. M. *Phys. Rev. B* **1995**, *51*, 8.

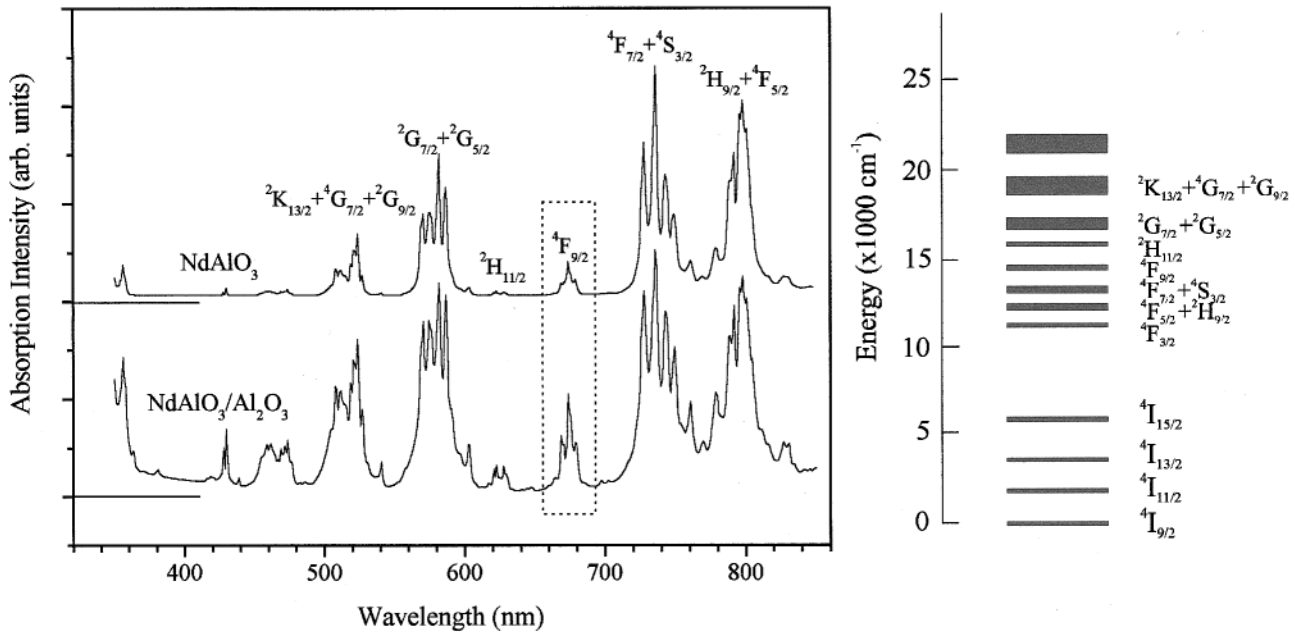

Figure 14. Room temperature UV−vis absorption spectra of $NdAlO_3$ and $NdAlO_3/Al_2O_3$.

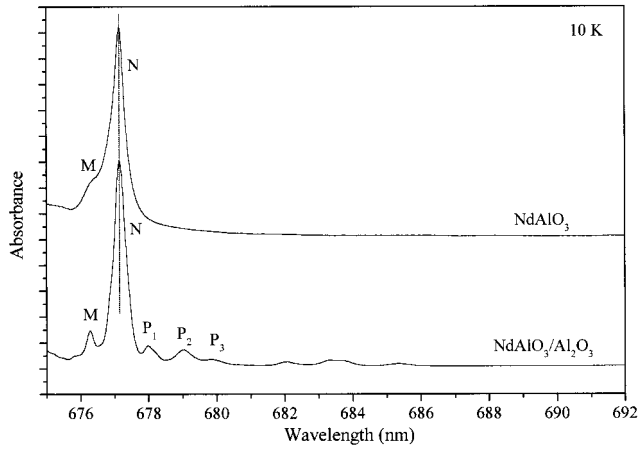

Figure 15. High-resolution absorption spectra ($^4I_{9/2}(1) \rightarrow {}^4F_{9/2}(1)$) of $NdAlO_3$ and $NdAlO_3/Al_2O_3$ obtained at 10 K.

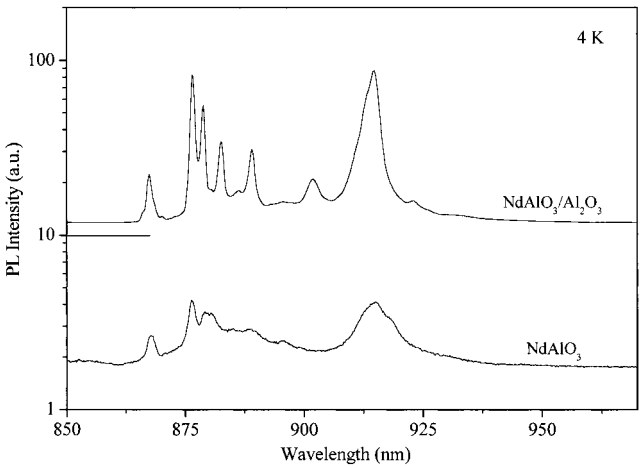

Figure 16. Photoluminescence spectra of Nd 4f $^4F_{3/2} \rightarrow {}^4I_{9/2}$ emission in the $NdAlO_3$ and $NdAlO_3/Al_2O_3$ systems.

nanoparticles are the source of nonradiative quenching sites in the luminescent materials, which decrease the luminescent intensity. In the composite material, the $NdAlO_3$ crystallites are in close contact with neighboring alumina grains (Figure 9b), which may compensate some of the surface defects and simultaneously act as a passivating medium to keep the neodymium aluminate centers effectively isolated (Scheme 2, I and II). On the other hand, the higher probability of $Nd^{3+}-Nd^{3+}$ contacts in the **NA** system results in a higher luminescence quenching efficiency (Figure 16). It has been observed that singly ionized oxygen vacancies, the so-called F^+ centers (+), exist in porous alumina, giving rise to a blue PL band near 450 nm.[64] Since the energy levels of F^+ centers are located in the band gap of alumina, the band gap decreases with increasing oxygen vacancies (Scheme 3). In view of the above, the larger background radiation observed near 350−400 nm in the $NdAlO_3/Al_2O_3$ composite can be due to the reduced absorption edge of nanoscaled alumina (Figure 14). Moreover, the concentration quenching among vicinal Nd centers, for example, those present in a single domain, is likely to be more favored compared to an intragranular cross-relaxation. If the $NdAlO_3/Al_2O_3$ composite is pumped, photons are also absorbed by the Al_2O_3 crystallites (including the F^+ center) to promote electrons from the conduction band (CB) to the valence band (VB). It can be expected that the energy released in the electron−hole recombination process in alumina is immediately reabsorbed by the adjacent Nd^{3+} centers; that is, the Al_2O_3 matrix transfers energy to the Nd ions. This process populates the excited state of Nd^{3+} additionally in the **NA3** sample, resulting ultimately in an enhancement of the luminescent efficiency.[65] On the contrary, the weak luminescence of pure $NdAlO_3$ can be assigned to concentration quenching by Nd ions and to "unrepaired" surface defects.

Conclusion

The compositionally different nanocomposites based on the dispersion of two or more solid phases are

(64) Du, Y.; Cai, W. L.; Mo, C. M.; Chen, J.; Zhang, L. D.; Zhu, X. G. *Appl. Phys. Lett.* **1999**, *74*, 2951.
(65) Park, J. K.; Ryu, H.; Park, H. D.; Choi, S. *J. Eur. Ceram. Soc.* **2001**, *21*, 535.

Scheme 2

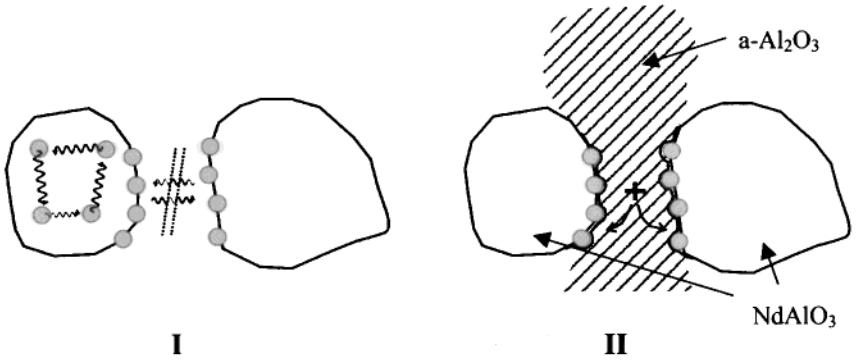

Scheme 3

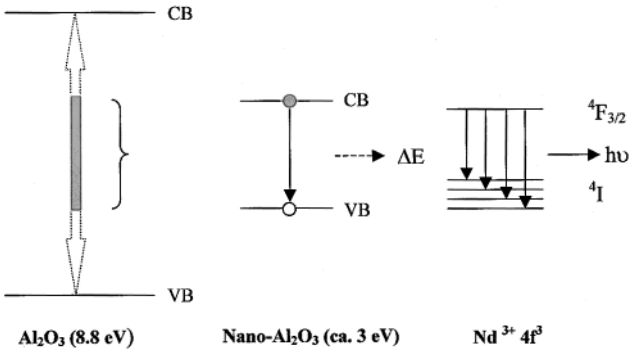

difficult to prepare by conventional preparation techniques, and phase segregation and agglomeration of particles commonly occur in the final material. The challenge of an intimate mixing of the discrete constituents can be achieved by combining the different elements required for the target ceramic or composite material in a single molecule. The single-stage sol−gel synthesis of a $NdAlO_3$ ceramic and a $NdAlO_3/Al_2O_3$ oxide−oxide composite, from chemically defined precursors, illustrates the potential of molecular level processing for obtaining nanoscaled materials. The principal conclusion to be drawn is that the heterometal alkoxides form gels by a controlled polymerization on hydrolysis without breaking down into separate constituents. Apparently, the retention of Nd−(O)−Al bridges in the gels is responsible for the easy and low-temperature conversion of green precursors to crystalline ceramic and composite. In the case of the composite formation, the phase separation takes place via the nucleation of $NdAlO_3$ embryos in a homogeneous $[\text{-Nd}-(\text{O})-\text{Al-}]_n$ mass, which, at high temperatures, results in a chemically imposed juxtaposition of the two ceramic phases to form a nano/nano composite.

The $LnAlO_3/Al_2O_3$ system described here can be defined as "glass-ceramics" representing a two-phase structure, where one phase is crystalline.[66] Glass-ceramics are noted for their unusual mix of properties, like increasing strength or extending the high-temperature use limits of the host glass. In general, the optical properties of such systems are ignored, largely because of the notion that scattering losses can never be small enough to make possible actual devices. But when the average sizes of the embedded crystallites and pores are smaller than the wavelength of the light and the refractive indices of the two phases are comparable, the scattering losses can be minimized. In our opinion, the ability of this novel composite to selectively partition a rare-earth phase in an amorphous matrix could lead to an interesting class of optical materials. The processing of these composites can offer materials with properties that are glasslike in most respects, except for the spectroscopy, where they act crystal-like. The final-stage sintering is generally accompanied by a rapid and excessive grain growth, due to which the advantages of the size effects are lost. The abnormal grain growth[67] in the **NA3** system suggests the possibility of obtaining fully dense material with nanosized grains.

Since the photoluminescence is remarkably enhanced (amplification: 35×) in the composite sample, it is reasonable to assume that the spatial separation of $NdAlO_3$ nanocrystals using an Al_2O_3 matrix is effective in reducing the concentration-quenching present in the pure $NdAlO_3$ phase, devoid of insulating neighbors. In addition, the singly ionized oxygen vacancies (F^+ centers) present in amorphous alumina may transfer the absorbed pump energy to the Nd centers. As a result, the Nd^{3+} ions, in **NA3**, also experience energy transfer from the excited alumina in addition to direct excitation. The nanodomains of neodymium aluminate separated from each other by the alumina matrix can be considered as "self-activated nanocrystals" (SANCs), whose efficiency has been enhanced by the matrix particles. Further, the dangling bonds of alumina clusters can bond to the large number of Nd atoms situated on the surface, thereby decreasing the defect density at the interface, in the composite material.

In summary, the restriction on the Nd−Nd separation within and on the surface of the $NdAlO_3$ nanocrystals, the $NdAlO_3-Al_2O_3$ interfaces, and the fact that the Al_2O_3 matrix acts as a spacer among the $NdAlO_3$ nanocrystals result in far less quenching of the luminescence than in the single-phase compound, where the close intergranular contacts adversely affect the luminescence efficiency.

Acknowledgment. The authors thank the Deutsche Forschungsgemeinschaft for supporting their work in the frame of research program Sonderforschungsbereich 277 (Grenzflaechenbestimmte Materialien) at the Saarland University, Saarbruecken. The Fonds der Chemis-

(66) Hench, L. L.; Noguès, J. L. In *Sol−Gel Optics Processing and Applications*; Klein, L. C., Ed.; Kluwer Academic: Dordrecht, 1993.

(67) Mayo, M. J. *Int. Mater. Rev.* **1996**, *41* (3), 85.

chen Industrie is also acknowledged for financial support. The Alexander von Humboldt Foundation, Germany, is gratefully acknowledged for a research fellowship to S.M. during 1994−96, when this work was initiated. We thank Prof. H. P. Beck and Ms. J. Bartelmus for the oxygen content analyses. We also acknowledge Mr. Thomas Agne for his assistance in the optical measurements.

CM0111433